

Nematicity and Magnetism in FeSe and other Families of Fe-based Superconductors

Youichi YAMAKAWA¹, Seiichiro ONARI², and Hiroshi KONTANI¹

¹ Department of Physics, Nagoya University, Furo-cho, Nagoya 464-8602, Japan.

² Department of Physics, Okayama University, Okayama 700-8530, Japan.

(Dated: May 17, 2019)

Nematicity and magnetism are two key features in Fe-based superconductors, and their interplay is one of the most important unsolved problems. In FeSe, the magnetic order is absent below the structural transition temperature $T_{\text{str}} = 90\text{K}$, in stark contrast that the magnetism emerges slightly below T_{str} in other families. To understand such amazing material dependence, we investigate the emergence of the nematic orbital-order ($n_{xz} \neq n_{yz}$) based on various first-principles Hubbard models. In Fe-based superconductors, spin-fluctuation-mediated large orbital-fluctuations appear because of the strong orbital-spin interplay due to the many-body effect. This effect is very significant in FeSe due to the small ratio between the Hund's and Coulomb interactions (\bar{J}/\bar{U}) and large d_{xz}, d_{yz} -orbitals weight at the Fermi level. For this reason, in FeSe, orbital order is established by weak spin fluctuations, so the magnetism is absent below T_{str} . In contrast, in LaFeAsO, the magnetic order appears just below T_{str} both experimentally and theoretically. Thus, the orbital-spin interplay is the key ingredient of the wide variety of the normal-state phase diagram in Fe-based superconductors.

Introduction

Amazing variety of the phase diagram in Fe-based superconductors, especially very unique normal state phase diagram in FeSe, offer us great hints to understand the fundamental electronic states. FeSe undergoes a structural and superconducting transitions at $T_{\text{str}} = 90\text{K}$ and $T_c = 8\text{K}$, respectively, whereas the magnetic transition is absent down to 0 K [1]. The strength of the antiferromagnetic (AFM) fluctuations is weak above T_{str} , while it starts to increase below T_{str} according to NMR study [2, 3] and neutron measurements [4, 5]. In stark contrast, the magnetic transition occurs at $T_{\text{mag}} \lesssim T_{\text{str}}$ in other undoped Fe-based superconductors. The main aim of this paper is to clarify the origin of the structure transition not accompanied by any magnetic order in FeSe.

Up to now, two promising triggers for the structure transition have been discussed intensively: In the spin-nematic scenario [6–9], the trigger is the spin-nematic order. This spin-fluctuation induced spin-quadrupole order could emerge above T_{mag} in highly magnetically frustrated systems. In the orbital order scenario [10–13], the trigger is the ferro-orbital (FO) order $n_{xz} \neq n_{yz}$. Above T_{str} , the strong orbital or spin-nematic fluctuations are observed by the measurements of shear modulus C_{66} [2, 14, 15], Raman spectroscopy [16–19], and in-plane resistivity anisotropy [20, 21]. The nematic orbital fluctuations originate from by the strong orbital-spin mode-coupling, which is microscopically described by the Aslamazov-Larkin vertex correction (AL-VC).

Except for the presence or absence of magnetism, FeSe and other Fe-based superconductors show common electronic properties. Below T_{str} , in both FeSe and BaFe₂As₂, large orbital polarization $\Delta E \equiv E_{yz} - E_{xz} \sim 50 \text{ meV}$ [22–29] is observed whereas the lattice distortion $(a - b)/(a + b)$ is just $0.2 \sim 0.3\%$ [2]. Above T_{str} , the electronic nematic susceptibility is enhanced in both

BaFe₂As₂ [14, 16, 20] and FeSe [2, 15], following the similar Curie-Weiss behavior. These facts indicate that the common microscopic mechanism drives the nematic order and fluctuations in all Fe-based superconductors, in spite of the presence or absence of the magnetism.

The goal of the present study is to explain the difference in the phase diagram between FeSe and other compounds on the same footing microscopically. For this purpose, we need the realistic multiorbital Hubbard model for each compound, which was already derived by using the first-principles method in Ref. [30]. To understand the absence of the magnetic order in FeSe, one significant hint is the smallness of the ratio between the Hund's and Coulomb interactions, \bar{J}/\bar{U} , since the Hund's coupling enlarges (suppresses) the intra-site magnetic (orbital) polarization. In fact, orbital fluctuations solely develop for smaller \bar{J}/\bar{U} in the analysis by the functional renormalization-group (fRG) theory [31, 32]. Another significant hint is the absence of the d_{xy} -orbital hole-pocket in FeSe, which is favorable for the orbital-spin interplay on the (d_{xz}, d_{yz}) -orbitals due to the AL-VC.

In this paper, we study the eight-orbital d - p Hubbard models for LaFeAsO and FeSe to understand the amazing variety of the normal-state phase diagrams. For this purpose, we study the spin-fluctuation-mediated orbital order by applying the self-consistent vertex-correction (SC-VC) method to the first-principles models. In FeSe, the orbital-spin interplay is significant because of the smallness of \bar{J}/\bar{U} and the absence of d_{xy} -hole pocket. For this reason, the orbital order is realized even when the spin fluctuations are substantially weak. On the other hand, in LaFeAsO, the orbital-spin interplay is relatively weak, so the orbital order is realized only when the spin fluctuations are very strong. We demonstrate that the rich variety of the phase diagrams in Fe-based superconductors, such as the presence or absence of the magnetic order below T_{str} , are well understood by analyzing the vertex

correction seriously. The SC-VC theory had been successfully applied to explain the complex phase diagram in H-doped LaFeAsO [33], nematic CDW order in under-doped cuprates [34, 35], and triplet superconductivity in Sr_2RuO_4 [32].

Model Hamiltonian and SC-VC theory

In the present study, we introduce the 8-orbital d - p Hubbard models H_{M}^0 for $\text{M} = \text{LaFeAsO}$ and FeSe , since the LDA multiorbital bandstructures are satisfactorily fitted in including not only five 3d orbitals on Fe, but also three 4p orbitals on As or Se. In addition, we use the Fe-site effective Coulomb interactions H_{M}^U given by the “constrained-RPA method” listed in TABLE XI of Ref. [30]. The averaged intra-orbital Coulomb interaction and Hund’s interaction on the d-orbitals are $(\bar{U}, \bar{J}) = (7.21, 0.681)$ [(4.23, 0.568)] in unit eV for FeSe [LaFeAsO]. Thus, the ratio $\bar{J}/\bar{U} = 0.0945$ in FeSe is much smaller than the ratio $\bar{J}/\bar{U} = 0.134$ in LaFeAsO and the ratios in other compounds, since the screening effect on U due to the valence bands not included in the d - p model is small in FeSe [30]. The relation $\bar{U} = \bar{U}' + 2/\bar{J}$ is approximately realized, where \bar{U}' is the averaged inter-orbital Coulomb interaction. Hereafter, we denote the five d-orbitals $d_{3z^2-r^2}, d_{xz}, d_{yz}, d_{xy}, d_{x^2-y^2}$ as 1, 2, 3, 4, 5, and three p-orbitals as 6 \sim 8.

The bandstructure and FSs for LaFeAsO tight-binding (TB) model are shown in Figs. 1 (a) and (b), respectively. Similar FSs with three hole-like FSs (h-FSs) and two electron-like FSs (e-FSs) are realized in many Fe-based superconductors. In FeSe , however, h-FS3 composed of d_{xy} -orbital is absent, and the size of each FS is very small as clarified by the ARPES studies [23, 27, 28] and dHvA studies [36, 37]. With these in mind, we introduce the additional intra-orbital hopping parameters into H_{FeSe}^0 , in order to shift the d_{xy} -orbital band [$d_{xz/yz}$ -orbital band] at $(\Gamma, \text{M}, \text{X})$ points by $(0, -0.25, +0.24)$ [$(-0.24, 0, +0.12)$] in unit eV. (see Supplementary Information.) These energy shifts might be induced by the self-energy [38]. The constructed bandstructure and FSs for FeSe are shown in Figs. 1 (a) and (c), respectively. Since each Fermi pocket is very shallow, the superconductivity in FeSe could be close to a BCS-BEC crossover [39].

In this article, we analyze the d - p Hubbard models $H_{\text{M}}(r) = H_{\text{M}}^0 + rH_{\text{M}}^U$ ($\text{M} = \text{LaFeAsO}, \text{FeSe}$) by applying the SC-VC method [13] using the Green function in Eq. (2). The ratio $J_{l,m}/U_{l,m}$ is unchanged by introducing the factor r [40, 41]. In addition, we introduce the constant mass-enhancement factor for d-orbital $1/z_l (\geq 1)$, which is included in the Green function (see Methods section). $1/z_l$ is given by the the self-energy as $1 - \partial\Sigma_{l,l}/\partial\epsilon|_{\epsilon=0}$. In the present study, r and z_l are the fitting parameters. We stress that essentially the same susceptibilities are

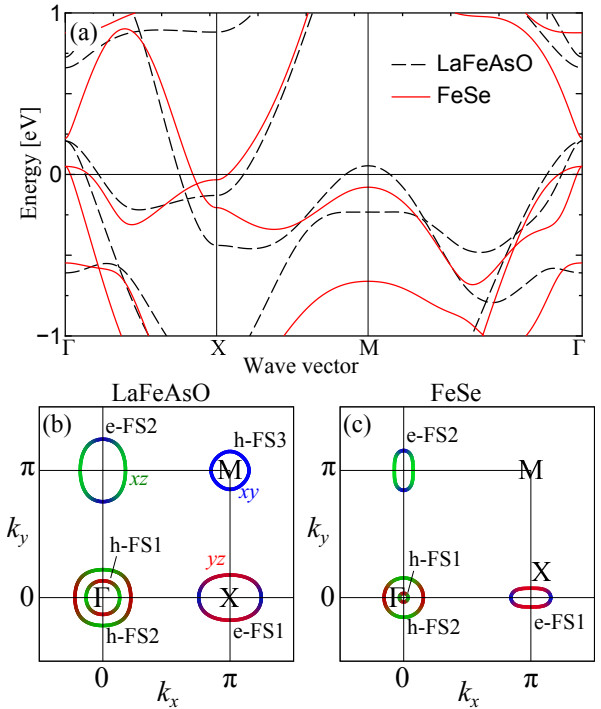


FIG. 1: **Bandstructures and FSs for LaFeAsO and FeSe .** (a) Bandstructures of the eight-orbital TB models for LaFeAsO and FeSe . (b) FSs for the LaFeAsO TB model. (c) FSs for the FeSe TB model. The colors correspond to 2 (green), 3 (red), and 4 (blue), respectively.

obtained for a fixed rz by setting the temperature as zT , as we will discuss later. In FeSe , the orbital order can be obtained in the real first-principles Hamiltonian ($r \approx 1$) by taking the experimental mass-enhancement factors $z_l^{-1} \approx 4$ into account.

In this article, we study the d-orbital charge (spin) susceptibilities (per spin), which is given in the following $5^2 \times 5^2$ matrix form:

$$\hat{\chi}^{c(s)}(\mathbf{q}) = \hat{\Phi}^{c(s)}(\mathbf{q})(1 - \hat{\Gamma}^{c(s)}\hat{\Phi}^{c(s)}(\mathbf{q}))^{-1} \quad (1)$$

where $\hat{\Phi}^{c(s)}(\mathbf{q}) = \hat{\chi}^0(\mathbf{q}) + \hat{X}^{c(s)}(\mathbf{q})$ is the irreducible susceptibility for the charge (spin) channel. We employ the AL-VC as \hat{X} , and the functional form for the AL-VC is explained in the Methods section. Hereafter, we mainly discuss the total spin susceptibility, $\chi^s(\mathbf{q}) \equiv \sum_{l,m} \chi_{l,l;m,m}^s(\mathbf{q})$, and the orbital susceptibilities for $O_{x^2-y^2} = n_{xz} - n_{yz}$, $\chi_{x^2-y^2}^c(\mathbf{q}) \equiv \chi_{2,2;2,2}^c(\mathbf{q}) + \chi_{3,3;3,3}^c(\mathbf{q}) - 2\chi_{2,2;3,3}^c(\mathbf{q})$. The divergence of $\chi_{x^2-y^2}^c(\mathbf{q})$ at $\mathbf{q} = \mathbf{0}$ gives rise to the FO order $n_{xz} \neq n_{yz}$. The charge (spin) Stoner factor $\alpha_{C(S)}$ is given by the maximum eigenvalue of $\hat{\Gamma}^{c(s)}\hat{\Phi}^{c(s)}(\mathbf{q})$ in Eq. (1), and the charge (spin) susceptibility is enlarged by the charge (spin) Stoner enhancement factor $S_{C(S)} \equiv (1 - \alpha_{C(S)})^{-1}$. Within the random-phase-approximation (RPA), only the spin fluctuations develop since the relation $\alpha_S > \alpha_C$ is satisfied for $J > 0$. However, the opposite relation

$\alpha_C > \alpha_S$ can be realized if the AL-VC is taken into account.

Numerical results for LaFeAsO and FeSe

First, we analyze the LaFeAsO model. The details of the analysis are found in Methods section. For $z = 1$ for each l , the obtained $\chi^s(\mathbf{q})$ and $\chi_{x^2-y^2}^c(\mathbf{q})$ are shown in Fig. 2 (a) and (b), respectively, for $r = 0.41$ ($\bar{U} = 1.74$ eV) at $T = 50$ meV. Thus, both AFM and FO susceptibilities develop divergently, and the realized enhancement factors are $S_S \approx 40$ and $S_C \approx 50$. The r -dependences of the enhancement factors at $T = 50$ meV are shown in the inset of Fig. 2 (c): Both S_S and S_C increase with r , and they are equivalent at $r^* = 0.41$. The lower the temperature is, the smaller r^* is, whereas the value of $S_S = S_C$ at r^* is approximately independent of T . Similar result is obtained in BaFe₂As₂ model as shown in Supplementary Information.

In addition, other antiferro-orbital susceptibilities $\chi_{xz}^c(\mathbf{q}) = 2[\chi_{3,4;3,4}^c(\mathbf{q}) + \chi_{3,4;4,3}^c(\mathbf{q})]$ and $\chi_{yz}^c(\mathbf{q}) = 2[\chi_{2,4;2,4}^c(\mathbf{q}) + \chi_{2,4;4,2}^c(\mathbf{q})]$ develop secondary as reported in previous studies [13, 33, 42]. The obtained results are essentially similar to the results obtained in the five d -orbital Hubbard model for LaFeAsO explained in Ref. [13].

Figure 2 (c) shows the temperature dependences of the Stoner enhancement factors at $r = 0.41$. Both S_C and S_S follow the Curie-Weiss behaviors with the spin and charge Weiss temperatures $\theta_C = 48$ meV and $\theta_S = 40$ meV, respectively. The obtained T -dependence of $\chi_{x^2-y^2}^c(\mathbf{0})$ is consistent with the experimental Curie-Weiss behavior of the nematic susceptibilities in BaFe₂As₂, derived from C_{66} [14, 15], Raman spectroscopy, [16, 17], and in-plane anisotropy of resistivity [20]. Since $\theta_C \sim \theta_S$, one could interpret that the orbital order in LaFeAsO is driven by the spin fluctuations.

Next, we analyze the FeSe model, in which the ratio \bar{J}/\bar{U} is considerably small. In FeSe, the experimental mass-enhancement factor m^*/m_b is ~ 10 for d_{xy} -orbital, and $3 \sim 4$ for other d -orbitals according to the ARPES study [23]. Taking such orbital-dependence of m^*/m_b into account, we put $z_l^{-1} = z^{-1}$ for $l \neq 4$ and $z_4^{-1} = 3z^{-1}$. In the RPA, $\chi^s(\mathbf{q})$ has the peak at $\mathbf{q} = (\pi, \pi)$ for $z_4^{-1} < 1.5$, whereas the peak moves to $\mathbf{q} = (\pi, 0)$ for $z_4^{-1} \geq 1.5$ consistently with experiments [5], and the results of the SC-VC method are essentially unchanged for $z_4^{-1} \geq 1.5$. We first study the case $z = 1$: Figures 3 (a) and (b) show the obtained $\chi^s(\mathbf{q})$ and $\chi_{x^2-y^2}^c(\mathbf{q})$ for $r = 0.25$ ($\bar{U} = 1.76$ eV) at $T = 50$ meV. Thus, only the FO susceptibility develop divergently [$S_C \approx 50$], whereas the AFM susceptibility remains small [$S_S \approx 8$], consistently with experiments for FeSe. We note that other FO susceptibility ($\chi_{z2}^c(\mathbf{q})$) and antiferro susceptibilities ($\chi_{xz/yz}^c(\mathbf{q})$) also develop secon-

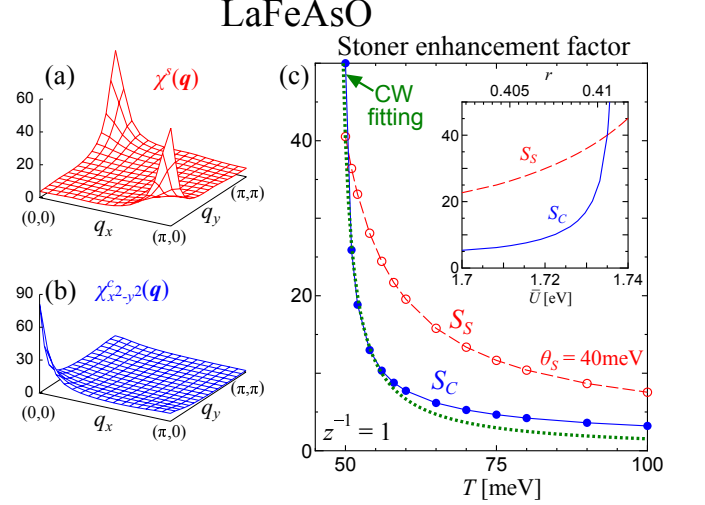


FIG. 2: Numerical results of the SC-VC theory for LaFeAsO. (a) $\chi^s(\mathbf{q})$ and (b) $\chi_{x^2-y^2}^c(\mathbf{q})$ obtained by the SC-VC method for LaFeAsO ($z = 1$). Note that other FO susceptibilities ($\chi_{z2}^c(\mathbf{q})$) and antiferro susceptibilities ($\chi_{xz/yz}^c(\mathbf{q})$) also develop secondarily. (c) Orbital (spin) enhancement factor $S_C(S)$ as function of T for LaFeAsO ($z = 1$) at $r = 0.41$. The charge and spin Weiss temperatures are $\theta_C = 48$ meV and $\theta_S = 40$ meV, respectively. Inset: $S_C(S)$ as function of r at $T = 50$ meV. Note that $\bar{U} = 4.23r$ eV for LaFeAsO.

darily, whereas $\chi_{xy}^c(\mathbf{0})$ and $\chi^c(\mathbf{0})$ (A_{1g} -mode) are not enhanced by the AL-VC. The r -dependences of the Stoner enhancement factors at $T = 50$ meV are shown in the inset of Fig. 3 (c): With increasing r , S_C increases rapidly whereas S_S remains small.

Figure 3 (c) shows the temperature dependences of the enhancement factors at $r = 0.25$. We stress that S_C follow the Curie-Weiss behavior with the Weiss temperature $\theta_C = 48$ meV: The obtained positive θ_C is consistent with the experimental Curie-Weiss behavior of the nematic susceptibility derived from C_{66} [2] and in-plane anisotropy of resistivity in FeSe. Since the spin Weiss temperature takes a large negative value ($\theta_S \sim -20$ meV), one may consider that the orbital order in FeSe stems from causes other than spin fluctuations.

Origin of the relation $S_C \gg S_S$ in FeSe

We discuss why the relation $S_C \gg S_S$ ($\theta_C > 0$ and $\theta_S < 0$) is obtained in FeSe in the present study. As we discuss in Methods section, the charge Stoner factor for $\chi_{x^2-y^2}^c(\mathbf{0})$ is $\alpha_C \approx (1 - 5J/U)(1 + UX^c)$, where X^c is the charge AL-VC for orbital 2 or 3. Since $\bar{J}/\bar{U} = 0.0945$ in FeSe, the orbital order is realized by relatively small AL-VC; $X^c \sim 0.9\chi^0(\mathbf{0})$. In LaFeAsO, in contrast, large AL-VC of order $\sim 2\chi^0(\mathbf{0})$ is required to realize the orbital order. The obtained AL-VCs in both systems are shown in Fig. 6 (c) in Supplementary Information.

Next, we discuss why the Curie-Weiss behavior of S_C is obtained in the FeSe model: As we discuss in Supplementary Information, the T -dependence of the AL-VC is given as $X^c \sim \Lambda^2 T S_S$, where Λ is the three-point vertex that represents the interference between two short-living magnons. $\Lambda^2 \propto T^{-a}$ with $a \approx 1$ at low temperatures due to the good nesting between h-FSSs and e-FSSs [17]. Thanks to the strong enhancement of Λ at low temperatures, the orbital order ($\alpha_C = 1$) is realized even if the spin Weiss temperature θ_S is negative. (Note that $T S_S$ decreases as $T \rightarrow 0$ when $\theta_S < 0$.) Thus, serious diagrammatic analysis of the AL-VC is necessary to understand the rich normal-state phase diagrams in Fe-bases superconductors.

In addition, the relation $\chi_{2(3)}^s(\mathbf{q}) \gg \chi_4^s(\mathbf{q})$ ($\chi_l^s(\mathbf{q}) \equiv \chi_{l,l,l,l}^s(\mathbf{q})$) is realized at the nesting vector in FeSe due to the absence of the d_{xy} -orbital h-FS (h-FS3). This condition is favorable for the development of $\chi_{x^2-y^2}^c(\mathbf{0})$ since $X_{2(3)}^c$ is enlarged by the spin fluctuations on the (d_{xz}, d_{yz}) -orbitals. To verify this consideration, in Fig. 3 (d), we show $\chi_{\max}^s \equiv \chi^s(\mathbf{Q})$ obtained for the FeSe model with $r = 0.25$, in addition to χ_{\max}^s and S_C obtained in the hybrid model $H_{\text{LaFeAsO}}^0 + rH_{\text{FeSe}}^U$ at $r = 0.232$. In both models, $\alpha_C = 0.98$ is satisfied at $T = 50$ meV, and S_C exhibits similar Curie-Weiss behavior for $T \geq 50$ meV, as shown in Figs. 3 (c) and (d). In the hybrid model with h-FS3, χ_{\max}^s takes a large value at the lowest temperature, consistently with the consideration at the beginning of this paragraph. Therefore, the absence of h-FS3 also contributes to realize the relation $\chi_{x^2-y^2}^c(\mathbf{0}) \gg \chi_{\max}^s$ in FeSe. More detailed analysis is given in Supplementary Information.

Effect of the mass-enhancement factor

Now, we study the FeSe model when the mass-enhancement factor for (d_{xz}, d_{yz}) -orbitals is $z^{-1} = 4$. The obtained $S_{C,S}$ as functions of r are shown in the inset of Fig. 3 (e) at $T = 12.5$ meV. Here, S_S remains small even for $r \sim 1$ since the bare susceptibility is multiplied by z . In contrast, $S_C \approx 50$ is realized for $r = 0.97$, which is very close to the exact first-principles Hubbard model $H_{\text{FeSe}}(r = 1)$. The T -dependences of $S_{C,S}$ are shown in Fig. 3 (e): Beautiful Curie-Weiss behavior with $\theta_C = 12$ meV is obtained by putting $r = 0.97$.

To understand the similarity between the results in Fig. 3 (c) for $z = 1$ and those in Fig. 3 (e) for $z^{-1} = 4$, we prove that both α_C and α_S are independent of z under the rescaling $T \rightarrow zT$ and $U \rightarrow z^{-1}U$, assuming that $z_l^{-1} = z^{-1}$ for any l for simplicity. Under this scaling, the Green function $\hat{G}(\mathbf{k}, n)$ at Matsubara integer n is independent of z , if the T -dependence of μ is negligible. For this reason, the bare susceptibility $\chi^0(\mathbf{q}) = -T \sum_{\mathbf{k}, n} G(\mathbf{k} + \mathbf{q}, n)G(\mathbf{k}, n)$ is scaled by z ,

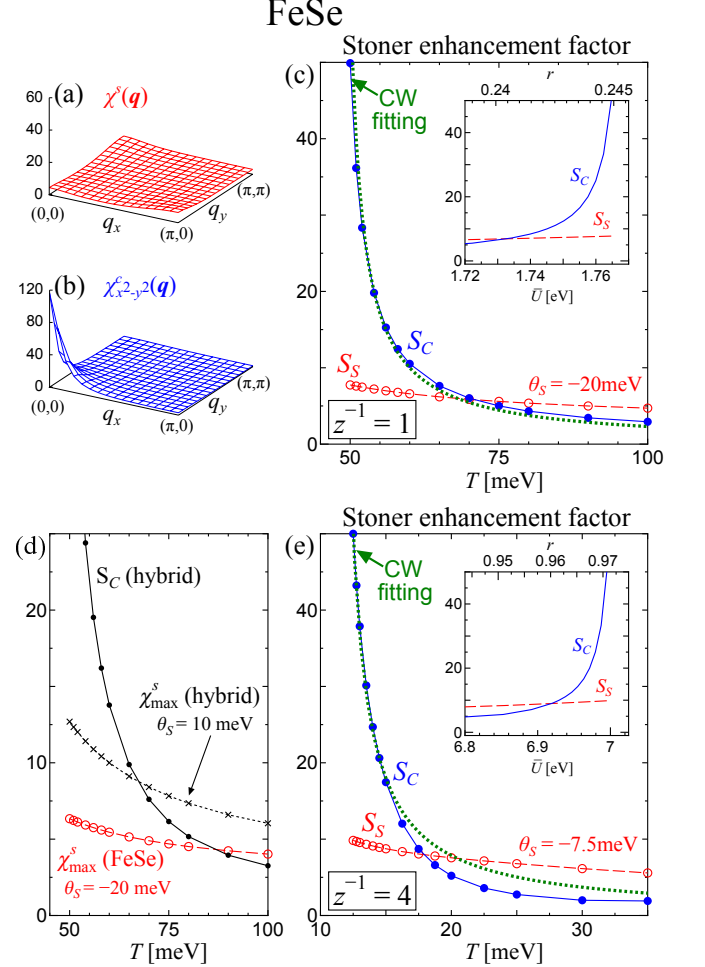


FIG. 3: Numerical results of the SC-VC theory for FeSe. (a) $\chi^s(\mathbf{q})$ and (b) $\chi_{x^2-y^2}^c(\mathbf{q})$ obtained by the SC-VC method for FeSe ($z = 1$), for $r = 0.25$ at $T = 50$ meV. (c) T -dependences of the Stoner enhancement factors for FeSe ($z = 1$) at $r = 0.25$. Note that $\bar{U} = 7.21r$ for FeSe. Inset: Stoner enhancement factors as function of r for FeSe ($z = 1$) at $T = 50$ meV. (d) χ_{\max}^s given by the SC-VC method for FeSe ($z = 1$). In comparison, we show χ_{\max}^s and S_C obtained for the hybrid model $H_{\text{LaFeAsO}}^0 + rH_{\text{FeSe}}^U$. (e) T -dependences of the enhancement factors for FeSe ($z = 4$) at $r = 0.97$. The charge and spin Weiss temperatures are $\theta_C = 12$ meV and $\theta_S \sim -7.5$ meV, respectively. Inset: Stoner enhancement factors as function of r for FeSe ($z = 4$) at $T = 12.5$ meV.

and therefore α_S is unchanged when U is rescaled by $z^{-1}U$. By following the same procedure, the AL-VC $X^c(\mathbf{0}) \sim TU^4 \sum_{\mathbf{q}} \Lambda(\mathbf{0}; \mathbf{q})^2 \chi^s(\mathbf{q})^2$ is scaled by z , since the three-point vertex Λ is scaled by z . As a result, α_C is unchanged under the rescaling of T and U . The validity of this scaling is confirmed in the insets of Figs. 3 (c) and (e).

Although we introduced the constant $z^{-1} = 4$ in calculating the susceptibilities in Fig. 3 (e), it is unnecessary if we calculate the self-energy $\hat{\Sigma}(k)$ as the function of $\hat{\chi}^{s,c}(q)$. In this case, fine tuning of r will be unneces-

sary since $\alpha_{S,C} < 1$ is assured if $\hat{\Sigma}(k)$ and $\hat{\chi}^{s,c}(q)$ are calculated self-consistently in two-dimensional systems (Mermin-Wagner theorem) [43]. This is our important future issue.

Spin fluctuation strength and k -dependent orbital-polarization below T_{str}

The FO order $n_{xz} \neq n_{yz}$ is established below the structure transition temperature T_{str} , at which the shear modulus C_{66} reaches zero. According to the linear-response theory, $C_{66} \propto 1 - g\chi_{x^2-y^2}^c(\mathbf{0})$, where $\chi_{x^2-y^2}^c(\mathbf{0}) \propto (T - \theta_C)^{-1}$ is the electronic orbital susceptibility given by the SC-VC theory, and g is the phonon-mediated Jahn-Teller energy [44]. Therefore, $C_{66} \propto (T - T_{\text{str}})/(T - \theta_C)$ and $T_{\text{str}} = \theta_C + g$. Since $g \approx 20 \sim 50$ K, T_{str} is slightly higher than θ_C due to weak acoustic e - ph coupling [2, 14, 15].

Next, we study the electronic states in the FO ordered state. Figure 4 (a) shows the T -dependence of S_S given by the RPA for LaFeAsO and FeSe for $z = 1$. Here, we introduce the orbital polarization by shifting the $d_{xz(yz)}$ -level by $-\Delta E/2$ ($\Delta E/2$). We put $S_S = 20$ (5) for LaFeAsO (FeSe) at $T_{\text{str}} = 50$ meV, and assume a mean-field-type T -dependence; $\Delta E = \Delta E_0 \tanh(1.74\sqrt{T_{\text{str}}/T - 1})$ with $\Delta E_0 = 80$ meV. (For $z^{-1} = 4$, the renormalized orbital polarization $z\Delta E_0$ is just below 20 meV.) In both LaFeAsO and FeSe, S_S are enhanced by ΔE , since α_S increases *linearly* with ΔE at $\mathbf{q} = (\pi, 0)$ as revealed in Ref. [44]. In LaFeAsO, the magnetic order temperature T_{mag} is increased to just below T_{str} since S_S is already large at T_{str} . In contrast, in FeSe, the enhancement of $\chi^s(\pi, 0)$ is much moderate [45]. Note that $\chi^s(\pi, 0)$ is enlarged even when ΔE is introduced only for the e-FSSs, as shown by the dot-dashed lines in Fig. 4 (a).

To verify the validity of Fig. 4 (a), we perform the self-consistent analysis of the orbital-polarization ($\Delta E_{xz}(\mathbf{k}), \Delta E_{yz}(\mathbf{k})$) and anisotropic $\chi^s(\mathbf{q})$, by extending the SC-VC theory for the ordered state [46]. In Fig. 4, we show the (b) FSs, (c) orbital polarization, and (d) $\chi^s(\mathbf{q})$ obtained in the FeSe model, in the case of $r = 0.243$ and $T = 50$ meV ($\alpha_S = 0.935$). The hole-pocket around Γ -point becomes ellipsoidal along the k_y -axis since $\Delta E_{xz} - \Delta E_{yz} > 0$ at $\mathbf{k} = \mathbf{0}$. Also, two Dirac-cone FSs appear around X-point due to $\Delta E_{yz}(\pi, 0) > 0$. These obtained FSs are consistent with the recent ARPES studies reported in Refs. [23–29]. Irrespective of the strong \mathbf{k} -dependence of the orbital polarization, $\chi^s(\mathbf{q})$ is enlarged at $\mathbf{q} \sim (\pi, 0)$ in Fig. 4 (d). In the present calculation, the AL-processes for the self-energy plays a crucial role. The detail of the theoretical study is presented in Ref. [46].

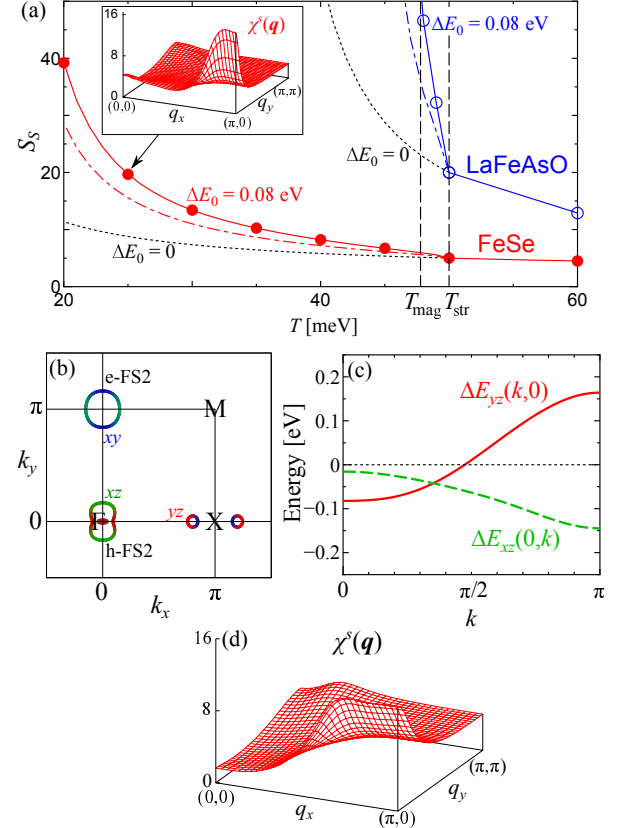


FIG. 4: Spin susceptibility and momentum dependence of the orbital polarization ($\Delta E_{xz}(\mathbf{k}), \Delta E_{yz}(\mathbf{k})$) below T_{str} . (a) T -dependences of S_S for LaFeAsO and FeSe ($z = 1$). The FO order is introduced below $T_{\text{str}} = 50$ meV. Inset: $\chi^s(\mathbf{q})$ for FeSe at $T = 25$ meV and $\Delta E_0 = 80$ meV without the renormalization. (b) FSs and (c) orbital polarization $\Delta E_{xz(yz)}(\mathbf{k})$ along the $k_{y(x)}$ -axis obtained by expanding the SC-VC theory for the ordered state in the FeSe model in the case of $\alpha_S = 0.935$. The shape of the C_2 -symmetric FSs in (b) is consistent with the experimental reports [23–29]. (d) C_2 -symmetric $\chi^s(\mathbf{q})$ in the orbital-ordered state.

Discussions

We studied the first-principles eight-orbital d - p Hubbard models for FeSe and LaFeAsO, and found that the spin-fluctuation-mediated orbital-order is realized in both systems thanks to the orbital-spin interplay given by the AL-VC. In FeSe, orbital order is established even when the spin fluctuations are very weak as shown in Fig. 3 (a)-(e), which is the main result of the present study. In stark contrast, the orbital order appears only in the vicinity of the SDW phase in the LaFeAsO model. In both models, the nematic orbital susceptibility follows the Curie-Weiss behavior $\propto (T - \theta_C)^{-1}$ with positive Weiss temperature: $\theta_C \gtrsim \theta_S$ for LaFeAsO, whereas $\theta_C \gg \theta_S$ ($\theta_S < 0$) for FeSe.

In explaining the orbital order in Fe-based superconductors, especially the orbital order without magnetiza-

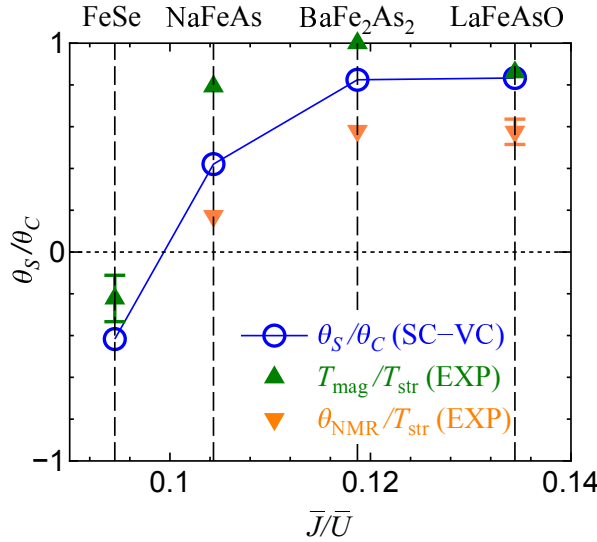


FIG. 5: The ratio θ_S/θ_C for FeSe, NaFeAs, BaFe₂As₂ and LaFeAsO as functions of \bar{J}/\bar{U} . Obtained θ_S/θ_C for four theoretical models. Experimental values of $T_{\text{mag}}/T_{\text{str}}$ and $\theta_{\text{NMR}}/T_{\text{str}}$ are also shown. θ_{NMR} is the Weiss temperature of $1/T_1 T$ obtained by the Curie-Weiss fitting for $T > T_{\text{str}}$ in LaFeAsO [47], BaFe₂As₂ [48], NaFeAs [49]. In LaFeAsO, we derived $\theta_{\text{NMR}} \approx 95$ K from the Curie-Weiss fitting of $1/T_1 T$ above T_{str} . In FeSe, we derived $T_{\text{mag}} = -10 \sim -30$ K from the Curie-Weiss fitting of $1/T_1 T$ below T_{str} [2]. The theoretically expected relationships $\theta_{\text{NMR}}/T_{\text{str}} \lesssim \theta_S/\theta_C$ and $T_{\text{mag}}/T_{\text{str}} \gtrsim \theta_S/\theta_C$ are verified.

tion in FeSe, the strong temperature dependence of the three-point vertex $\Lambda^2 \propto T^{-a}$ ($a \approx 1$) due to the good nesting between h-FSSs and e-FSSs [17] plays a crucial role. Therefore, serious numerical study of the VC is necessary to understand the rich variety of the normal-state phase diagram in Fe-based superconductors.

The ratio θ_S/θ_C obtained in FeSe, NaFeAs, BaFe₂As₂, and LaFeAsO are summarized in Fig. 5, as function of \bar{J}/\bar{U} . Numerical study for NaFeAs and BaFe₂As₂ are presented in the Supplementary Information. In NaFeAs and FeSe, in which \bar{J}/\bar{U} is smaller, the obtained θ_S/θ_C decreases to 0.4 and -0.4, respectively. Experimental values of $T_{\text{mag}}/T_{\text{str}}$ and $\theta_{\text{NMR}}/T_{\text{str}}$ are also shown, where θ_{NMR} is the Weiss temperature of $1/T_1 T$ above T_{str} . Since $T_{\text{str}} = \theta_C + g$ and $\theta_{\text{NMR}} = \theta_S$, the relation $\theta_{\text{NMR}}/T_{\text{str}} \lesssim \theta_S/\theta_C$ is expected theoretically. In addition, the relation $T_{\text{mag}}/T_{\text{str}} \gtrsim \theta_S/\theta_C$ is expected since T_{mag} is substantially higher than θ_S due to the FO order in the orthorhombic phase. These two theoretically predicted relations are verified in Fig. 5.

In the present study, we neglected the spin-channel VCs for simplicity. The validity of this simplification is verified in Supplementary Information, by performing a time-consuming self-consistent calculation with respect to both charge- and spin-channel Maki-Thompson (MT) and AL-VCs.

The pairing mechanism in Fe-based superconductors is our important future problem. In FeSe, T_c increases from 9 K to 40 K under pressure, accompanied by the enhancement of spin fluctuations. At the same time, the system approaches to the orbital critical point since T_{str} decreases to zero under pressure. These facts indicate the important roles of spin and orbital fluctuations [50] on the pressure-induced high- T_c state in FeSe.

Methods

Here, we explain the outline of the present numerical study based on the SC-VC theory. The Green function in the present eight-orbital Hubbard model is given as the following 8×8 matrix form in the orbital basis:

$$\hat{G}(k) = (\hat{z}^{-1}i\epsilon_n + \mu - \hat{h}_M^0(\mathbf{k}))^{-1}, \quad (2)$$

where $k = (\mathbf{k}, \epsilon_n = (2n + 1)\pi T)$, $\hat{h}_M^0(\mathbf{k})$ is the kinetic term ($M = \text{FeSe}$ or LaFeAsO), and $\hat{z}^{-1} \equiv 1 - \partial\hat{\Sigma}/\partial\epsilon|_{\epsilon=0}$ represents the mass-enhancement due to the self-energy at the Fermi level. Equation (2) gives the coherent part of the Green function, which mainly determines the low-energy electronic properties. We assume \hat{z}^{-1} is diagonal, and $(\hat{z}^{-1})_{l,l} \equiv 1/z_l$ for $l = 1 \sim 5$, and $(\hat{z}^{-1})_{l,l} = 1$ for $l = 6 \sim 8$.

The d -orbital charge and spin susceptibilities are given in the $5^2 \times 5^2$ matrix form in Eq. (1), using the irreducible charge and spin susceptibilities $\hat{\Phi}^{c,s}(\mathbf{q}) = \hat{\chi}^0(\mathbf{q}) + \hat{X}^{c,s}(\mathbf{q})$. In the SC-VC theory, we employ the AL-VC as $\hat{X}^{c,s}(\mathbf{q})$, and perform the self-consistent calculation with respect to the AL-VC and susceptibilities. Using the Green function in Eq. (2), the bare susceptibility is

$$\chi_{l,l';m,m'}^0(q) = -T \sum_k G_{l,m}(k+q) G_{m',l'}(k), \quad (3)$$

where $q = (\mathbf{q}, \omega_l = 2l\pi T)$. Also, the AL-VC for the charge susceptibility is given as

$$\begin{aligned} X_{l,l';m,m'}^{\text{AL},c}(q) &= \frac{T}{2} \sum_p \sum_{a \sim h} \Lambda_{l,l';a,b;e,f}(q; p) \\ &\times \{3V_{a,b;c,d}^s(p+q)V_{e,f;g,h}^s(-p) + V_{a,b;c,d}^c(p+q)V_{e,f;g,h}^c(-p)\} \\ &\times \Lambda'_{m,m';c,d;g,h}(q; p), \end{aligned} \quad (4)$$

where $p = (\mathbf{p}, \omega_m)$, and $\hat{V}^{s,c}(q) \equiv \hat{\Gamma}^{s,c} + \hat{\Gamma}^{s,c}\hat{\chi}^{s,c}(q)\hat{\Gamma}^{s,c}$. The three-point vertex $\hat{\Lambda}(q; p)$ is given as

$$\Lambda_{l,l';a,b;e,f}(q; p) = -T \sum_{k'} G_{l,a}(k'+q) G_{f,l'}(k') G_{b,e}(k'-p), \quad (5)$$

and $\Lambda'_{m,m';c,d;g,h}(q; p) \equiv \Lambda_{c,h;m,g;d,m'}(q; p) + \Lambda_{g,d;m,c;h,m'}(q; -p - q)$. We include all U^2 -terms without the double counting in order to obtain quantitatively reliable results. Equation (4) means that the charge AL-VC becomes large in the presence of

strong spin fluctuations. More detailed explanations are presented in the textbook [42].

In the present study, we neglect the spin-channel VC since it is not important as discussed in Ref. [51]. The smallness of the spin-channel VC in the FeSe model is verified in Supplementary Information.

As explained in Ref. [51], the development of $\chi_{x^2-y^2}^c(\mathbf{0})$ is mainly caused by the diagonal elements of $\hat{\Phi}^c$ with respect to $l = 2, 3$. If we drop the off-diagonal elements of $\hat{\Phi}^c$ approximately, $\chi_{x^2-y^2}^c(\mathbf{0})$ is given as [51],

$$\chi_{x^2-y^2}^c(\mathbf{0}) \approx 2\Phi^c/(1 - (1 - 5J/U)U\Phi^c), \quad (6)$$

where $U \equiv U_{2,2} = U_{3,3}$, $J \equiv J_{2,3}$, $\Phi^c \equiv \chi_{l,l;l,l}^0(\mathbf{0}) + X_{l,l;l,l}^c(\mathbf{0})$ ($l = 2$ or 3). Thus, the charge Stoner factor is $\alpha_C = (1 - 5J/U)U\Phi^c \approx (1 - 5J/U)(1 + UX^c)$, considering the relation $\chi^0(\mathbf{q}) \approx 1/U$.

Acknowledgments:

We are grateful to A. Chubukov, P.J. Hirschfeld, R. Fernandes, J. Schmalian, Y. Matsuda, and T. Shimojima for useful discussions. This study has been supported by Grants-in-Aid for Scientific Research from MEXT of Japan.

[1] Johnston, D. C. The puzzle of high temperature superconductivity in layered iron pnictides and chalcogenides. *Adv. Phys.* **59**, 803-1061 (2010); Mizuguchi, Y. & Takano, Y. Review of Fe Chalcogenides as the Simplest Fe-Based Superconductor. *J. Phys. Soc. Jpn.* **79**, 102001 (2010).

[2] Böhmer, A. E. *et al.* Origin of the Tetragonal-to-Orthorhombic Phase Transition in FeSe: A Combined Thermodynamic and NMR Study of Nematicity. *Phys. Rev. Lett.* **114**, 027001 (2015).

[3] Baek, S.-H. *et al.* Orbital-driven nematicity in FeSe. *Nature Mater.* **14**, 210-214 (2015).

[4] Rahn, M. C., Ewings, R. A., Sedlmaier, S. J., Clarke, S. J. & Boothroyd, A. T. Strong $(\pi, 0)$ spin fluctuations in β -FeSe observed by neutron spectroscopy. *Phys. Rev. B* **91**, 180501(R) (2015).

[5] Wang, Q. *et al.* Strong Interplay between Stripe Spin Fluctuations, Nematicity and Superconductivity in FeSe. Preprint at <http://arxiv.org/abs/1502.07544> (2015).

[6] Fernandes, R. M. *et al.* Effects of Nematic Fluctuations on the Elastic Properties of Iron Arsenide Superconductors. *Phys. Rev. Lett.* **105**, 157003 (2010).

[7] Wang, F., Kivelson, S. & Lee, D.-H. Is FeSe a nematic quantum paramagnet? Preprint at <http://arxiv.org/abs/1501.00844> (2015).

[8] Chubukov, A. V., Fernandes, R. M. & Schmalian, J. Origin of nematic order in FeSe. *Phys. Rev. B* **91**, 201105(R) (2015).

[9] Glasbrenner, J. K. *et al.* Effect of magnetic frustration on nematicity and superconductivity in iron chalcogenides. *Nature Physics advance online publication*, (2015).

[10] Krüger, F., Kumar, S., Zaanen, J. & van den Brink, J. Spin-orbital frustrations and anomalous metallic state in iron-pnictide superconductors. *Phys. Rev. B* **79**, 054504 (2009).

[11] Lv, W., Wu, J. & Phillips, P. Orbital ordering induces structural phase transition and the resistivity anomaly in iron pnictides. *Phys. Rev. B* **80**, 224506 (2009).

[12] Lee, C.-C., Yin, W.-G. & Ku, W. Ferro-Orbital Order and Strong Magnetic Anisotropy in the Parent Compounds of Iron-Pnictide Superconductors. *Phys. Rev. Lett.* **103**, 267001 (2009).

[13] Onari, S. & Kontani, H. Self-consistent Vertex Correction Analysis for Iron-based Superconductors: Mechanism of Coulomb Interaction-Driven Orbital Fluctuations. *Phys. Rev. Lett.* **109**, 137001 (2012).

[14] Yoshizawa, M. *et al.* Structural Quantum Criticality and Superconductivity in Iron-Based Superconductor $\text{Ba}(\text{Fe}_{1-x}\text{Co}_x)_2\text{As}_2$. *J. Phys. Soc. Jpn.* **81**, 024604 (2012).

[15] Böhmer, A. E. *et al.* Nematic Susceptibility of Hole-Doped and Electron-Doped BaFe_2As_2 Iron-Based Superconductors from Shear Modulus Measurements. *Phys. Rev. Lett.* **112**, 047001 (2014).

[16] Gallais, Y. *et al.* Observation of Incipient Charge Nematicity in $\text{Ba}(\text{Fe}_{1-x}\text{Co}_x)_2\text{As}_2$. *Phys. Rev. Lett.* **111**, 267001 (2013).

[17] Kontani, H. & Yamakawa, Y. Linear Response Theory for Shear Modulus C_{66} and Raman Quadrupole Susceptibility: Evidence for Nematic Orbital Fluctuations in Fe-based Superconductors. *Phys. Rev. Lett.* **113**, 047001 (2014).

[18] Khodas, M. & Levchenko, A. Raman scattering as a probe of nematic correlations. *Phys. Rev. B* **91**, 235119 (2015).

[19] Karahasanovic, U. *et al.* Manifestation of nematic degrees of freedom in the Raman response function of iron pnictides. Preprint at <http://arxiv.org/abs/1504.06841> (2015).

[20] Chu, J.-H., Kuo, H.-H., Analytis, J. G. & Fisher, I. R. Divergent Nematic Susceptibility in an Iron Arsenide Superconductor. *Science* **337**, 710-712 (2012).

[21] H.-H. Kuo, J.-H. Chu, S.A. Kivelson, and I.R. Fisher, arXiv:1503.00402.

[22] Yi, M. *et al.* Symmetry-breaking orbital anisotropy observed for detwinned $\text{Ba}(\text{Fe}_{1-x}\text{Co}_x)_2\text{As}_2$ above the spin density wave transition. *Proc. Natl. Acad. Sci. USA* **108**, 6878-6883 (2011).

[23] Maletz, J. *et al.* Unusual band renormalization in the simplest iron-based superconductor FeSe_{1-x} . *Phys. Rev. B* **89**, 220506(R) (2014).

[24] Nakayama, K. *et al.* Reconstruction of Band Structure Induced by Electronic Nematicity in an FeSe Superconductor. *Phys. Rev. Lett.* **113**, 237001 (2014).

[25] Shimojima, T. *et al.* Lifting of zx/yz orbital degeneracy at the structural transition in detwinned FeSe. *Phys. Rev. B* **90**, 121111 (2014).

[26] Zhang, P. *et al.* Observation of two distinct d_{xz}/d_{yz} band splittings in FeSe. *Phys. Rev. B* **91**, 214503 (2015).

[27] Zhang, Y. *et al.* Distinctive momentum dependence of the band reconstruction in the nematic state of FeSe thin film. Preprint at <http://arxiv.org/abs/1503.01556> (2015).

[28] Suzuki, Y. *et al.* Momentum-dependent sign-inversion of orbital polarization in superconducting FeSe. Preprint at <http://arxiv.org/abs/1504.00980> (2015).

[29] Watson, M. D. *et al.* Suppression of orbital order-

ing by chemical pressure in $\text{FeSe}_{1-x}\text{S}_x$. Preprint at <http://arxiv.org/abs/1508.05016> (2015).

[30] T. Miyake, K. Nakamura, R. Arita, and M. Imada, *J. Phys. Soc. Jpn.* **79**, 044705 (2010). Miyake, T., Nakamura, K., Arita, R. & Imada, M. Comparison of Ab initio Low-Energy Models for LaFePO , LaFeAsO , BaFe_2As_2 , LiFeAs , FeSe , and FeTe : Electron Correlation and Covacency. *J. Phys. Soc. Jpn.* **79**, 044705 (2010).

[31] Tsuchiizu, M., Ohno, Y., Onari, S. & Kontani, H. Orbital Nematic Instability in the Two-Orbital Hubbard Model: Renormalization-Group + Constrained RPA Analysis. *Phys. Rev. Lett.* **111**, 057003 (2013).

[32] Tsuchiizu, M., Yamakawa, Y., Onari, S., Ohno, Y. & Kontani, H. Spin-triplet superconductivity in Sr_2RuO_4 due to orbital and spin fluctuations: Analyses by two-dimensional renormalization group theory and self-consistent vertex-correction method. *Phys. Rev. B* **91**, 155103 (2015).

[33] Onari, S., Yamakawa, Y. & Kontani, H. High- T_c Superconductivity near the Anion Height Instability in Fe-Based Superconductors: Analysis of $\text{LaFeAsO}_{1-x}\text{H}_x$. *Phys. Rev. Lett.* **112**, 187001 (2014).

[34] Yamakawa, Y. & Kontani, H. Spin-Fluctuation-Driven Nematic Charge-Density Wave in Cuprate Superconductors: Impact of Aslamazov-Larkin Vertex Corrections. *Phys. Rev. Lett.* **114**, 257001 (2015).

[35] Tsuchiizu, M., Yamakawa, Y. & Kontani, H. p -Orbital Density Wave with d Symmetry in High- T_c Cuprate Superconductors: Preprint at <http://arxiv.org/abs/1508.07218> (2015).

[36] Terashima, T. *et al.* Anomalous Fermi surface in FeSe seen by Shubnikov-de Haas oscillation measurements. *Phys. Rev. B* **90**, 144517 (2014).

[37] Audouard, A. *et al.* Quantum oscillations and upper critical magnetic field of the iron-based superconductor FeSe . *Europhys. Lett.* **109**, 27003 (2015).

[38] Yin, Z. P., Haule, K. & Kotliar, G. Kinetic frustration and the nature of the magnetic and paramagnetic states in iron pnictides and iron chalcogenides. *Nature Mater.* **10**, 932-935 (2011); Ferber, J., Foyevtsova, K., Valentí, R. & Jeschke, H. O. LDA + DMFT study of the effects of correlation in LiFeAs . *Phys. Rev. B* **85**, 094505 (2012); Lee, G. *et al.* Orbital Selective Fermi Surface Shifts and Mechanism of High T_c Superconductivity in Correlated $A\text{FeAs}$ ($A = \text{Li}, \text{Na}$). *Phys. Rev. Lett.* **109**, 177001 (2012).

[39] Kasahara, S. *et al.* Field-induced superconducting phase of FeSe in the BCS-BEC cross-over. *Proc. Natl. Acad. Sci. USA* **111**, 16309-16313 (2014).

[40] Suzuki, K., Usui, H. & Kuroki, K. Possible Three-Dimensional Nodes in the $s\pm$ Superconducting Gap of $\text{BaFe}_2(\text{As}_{1-x}\text{P}_x)_2$. *J. Phys. Soc. Jpn.* **80**, 013710 (2011).

[41] Misawa, T. & Imada, M. Superconductivity and its mechanism in an ab initio model for electron-doped LaFeAsO . *Nature Commun.* **5**, 5738 (2014).

[42] Onari, S. & Kontani, H. *Iron-Based Superconductivity*, (ed. Johnson, P. D., Xu, G. & Yin, W.-G. Springer-Verlag Berlin and Heidelberg GmbH & Co. K (2015)).

[43] Kontani, H. & Ohno, M. Effect of a nonmagnetic impurity in a nearly antiferromagnetic Fermi liquid: Magnetic correlations and transport phenomena. *Phys. Rev. B* **74**, 014406 (2006).

[44] Kontani, H., Saito, T. & Onari, S. Origin of orthorhombic transition, magnetic transition, and shear-modulus softening in iron pnictide superconductors: Analysis based on the orbital fluctuations theory. *Phys. Rev. B* **84**, 024528 (2011).

[45] Mukherjee, S., Kreisel, A., Hirschfeld, P. J. & Andersen, B. M. Model of Electronic Structure and Superconductivity in Orbitally Ordered FeSe . *Phys. Rev. Lett.* **115**, 026402 (2015).

[46] Onari, S., Yamakawa, Y. & Kontani, H., arXiv:1509.

[47] Nakai, Y. *et al.* Enhanced anisotropic spin fluctuations below tetragonal-to-orthorhombic transition in $\text{LaFeAs}(\text{O}_{1-x}\text{F}_x)$ probed by ^{75}As and ^{139}La NMR. *Phys. Rev. B* **85**, 134408 (2012).

[48] Ning, F. L. *et al.* Contrasting Spin Dynamics between Underdoped and Overdoped $\text{Ba}(\text{Fe}_{1-x}\text{Co}_x)_2\text{As}_2$. *Phys. Rev. Lett.* **104**, 037001 (2010).

[49] Ma, L. *et al.* ^{23}Na and ^{75}As NMR study of antiferromagnetism and spin fluctuations in NaFeAs single crystals. *Phys. Rev. B* **83**, 132501 (2011).

[50] Kontani, H. & Onari, S. Orbital-Fluctuation-Mediated Superconductivity in Iron Pnictides: Analysis of the Five-Orbital Hubbard-Holstein Model. *Phys. Rev. Lett.* **104**, 157001 (2010).

[51] Ohno, Y., Tsuchiizu, M., Onari, S. & Kontani, H. Spin-Fluctuation-Driven Orbital Nematic Order in Ru-Oxides: Self-Consistent Vertex Correction Analysis for Two-Orbital Model. *J. Phys. Soc. Jpn.* **82**, 013707 (2012).

[Supplementary Information]
Nematicity and Magnetism in FeSe and other Families of Fe-based Superconductors

Youichi Yamakawa¹, Seiichiro Onari², and Hiroshi Kontani¹

¹ Department of Physics, Nagoya University, Nagoya 464-8602, Japan

² Department of Physics, Okayama University, Okayama 700-8530, Japan

Why strong orbital fluctuations are induced by tiny spin fluctuations in FeSe?

In the main text, we derived the first principles 8-orbital d - p Hubbard models for LaFeAsO and FeSe. The bandstructures and Fermi surfaces are shown in Fig. 1 in the main text. In FeSe, we introduce the intra-orbital hopping parameters into H_{FeSe}^0 in order to shift the d_{xy} -orbital band [d_{xz}/yz -orbital band] at (Γ, M, X) points by $(0, -0.25, +0.24)$ [$(-0.24, 0, +0.12)$] in unit eV. Such level shifts are introduced by the additional intra-orbital hopping integrals; $\delta t^{\text{on-site}} = \delta E_{\Gamma}/4 + \delta E_M/4 + \delta E_X/2$, $\delta t^{\text{nn}} = \delta E_{\Gamma}/8 - \delta E_M/8$, and $\delta t^{\text{nnn}} = \delta E_{\Gamma}/16 + \delta E_M/16 - \delta E_X/8$.

By applying the SC-VC method to these models, it is found that the ferro-orbital order ($n_{xz} \neq n_{yz}$) is induced by the AL-VC in both compounds. The obtained spin and orbital susceptibilities, $\chi_{\text{max}}^s \equiv \chi^s(\mathbf{Q})$ and $\chi_{x^2-y^2}^c(\mathbf{0}) \equiv \chi_{2,2;2,2}^c(\mathbf{q}) + \chi_{3,3;3,3}^c(\mathbf{q}) - 2\chi_{2,2;3,3}^c(\mathbf{0})$ are shown in Figs. 6 (a) and (b), respectively. In both FeSe and LaFeAsO, the charge Stoner factor is $\alpha_C = 0.98$ at $T = 50$ meV, and the obtained orbital susceptibilities show similar T -dependence. We set $\bar{U} = 1.76$ ($r = 0.25$) in FeSe, and $\bar{U} = 1.74$ ($r = 0.41$) in LaFeAsO, as we did in the main text. As for the spin susceptibility, in LaFeAsO, strong spin fluctuations develop at $T = 50$ meV ($\alpha_S = 0.98$), consistently with previous theoretical studies [13, 33]. In FeSe, in contrast, χ_{max}^s is almost constant till $T = 50$ meV ($\alpha_S = 0.87$), consistently with experimental reports in FeSe.

Now, we discuss the reason why the spin fluctuation strength required to realize $\alpha_C \approx 1$ is so different from LaFeAsO to FeSe. One reason is the difference in the ratio \bar{J}/\bar{U} : Figure 6 (c) shows the T -dependence of the AL-VC on d_{xz} -orbital, $X_2^{\text{AL},c}(\mathbf{0}) \equiv X_{2,2;2,2}^{\text{AL},c}(\mathbf{0})$, obtained for LaFeAsO and FeSe at $T = 50$ meV ($\alpha_C = 0.98$). At $T = 50$ meV, the AL-VC for FeSe is about one-half of that in LaFeAsO. Thus, small AL-VC is enough to induce large orbital fluctuations in FeSe, since the charge Stoner factor is $\alpha_C \approx (1 - 5\bar{J}/\bar{U})\bar{U}\Phi_2^c(\mathbf{0})$.

In Fig. 6 (d), we show that $X_2^{\text{AL},c: \text{non-zero}}(\mathbf{0}) \equiv X_2^{\text{AL},c}(\mathbf{0}) - X_2^{\text{AL},c: \text{zero}}(\mathbf{0})$ is very small for both FeSe and LaFeAsO. Here, “zero” represents the zero-Matsubara term (classical contribution) in eq. (4) in Methods section. Thus, non-zero Matsubara terms in the AL-VC are negligible in the present calculation (by chance). Note

that the U^2 -term in AL-VC gives negative contribution.

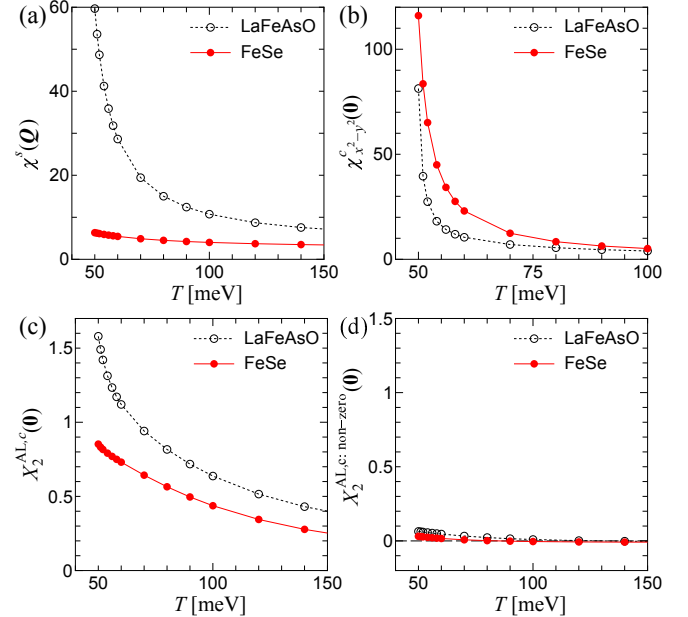


FIG. 6: Spin and orbital susceptibilities, and Aslamazov-Larkin vertex corrections. (a) Spin susceptibility $\chi^s(\mathbf{Q})$ and (b) orbital susceptibilities $\chi_{x^2-y^2}^c(\mathbf{0})$ for FeSe and LaFeAsO as functions of T . We put $r = 0.25$ for FeSe, and $r = 0.41$ for LaFeAsO. (c) $X_2^{\text{AL},c}(\mathbf{0})$ and (d) $X_2^{\text{AL},c: \text{non-zero}}(\mathbf{0})$ for FeSe and LaFeAsO.

Another reason for the relation $\chi_{\text{max}}^s(\text{FeSe}) \ll \chi_{\text{max}}^s(\text{LaFeAsO})$ at $\alpha_C \approx 1$ is the difference in the orbital dependence of the spin fluctuation strength: The AL-VC for the xz -orbital is approximately given as

$$X_2^{\text{AL},c}(\mathbf{0}) \approx 3TU^4 \sum_{\mathbf{k}} |\Lambda_{2,2;2,2}(\mathbf{0}; \mathbf{k})|^2 \chi_2^s(\mathbf{k})^2 \quad (7)$$

where we dropped the inter-orbital terms of $\hat{\chi}^s$ and $\hat{\Lambda}$, and leave only the zero-Matsubara term in the Matsubara summation in eq. (4) in Methods section. If Eq. (7) is justified, only the spin fluctuations on (d_{xz}, d_{yz}) -orbitals are important for the FO fluctuations.

Figure 7 (a) shows $\chi_2^s(\mathbf{Q})$ for FeSe and LaFeAsO for the same model parameters used in Fig. 6. As derived from Fig. 6 (a) and Fig. 7 (a), the ratio $\chi_2^s(\mathbf{Q})/\chi^s(\mathbf{Q})$ is 0.22 in LaFeAsO, whereas the ratio increases to 0.53 in FeSe, since the relation $\chi_4^s(\mathbf{Q}) \ll \chi_2^s(\mathbf{Q})$ ($\chi_4^s(\mathbf{Q}) \sim \chi_2^s(\mathbf{Q})$) is

satisfied in FeSe (LaFeAsO) because of the absence (presence) of h-FS3. This orbital dependence of the spin fluctuations in FeSe is favorable for realizing the FO fluctuations.

To understand the AL-VC due to spin fluctuations in more detail, we calculate $C_2 \equiv \sum_{\mathbf{q}} \chi_2^s(\mathbf{q})^2$ and show the result in Fig. 7 (b): The ratio $C_2^{\text{LaFeAsO}}/C_2^{\text{FeSe}}$ is just 1.35 since the width of the peak of $\chi_2^s(\mathbf{q})^2$ around $\mathbf{q} = \mathbf{Q}$ is much wider in FeSe. We also examine the square of the three-point vertex for d_{xz} -orbital $\Lambda_2 \equiv \Lambda_{2,2;2,2;2,2}(\mathbf{q}, \mathbf{k})$ at $\mathbf{q} = \mathbf{0}$ and $\mathbf{k} = \mathbf{Q}$ in Fig. 7 (c). In both models, the relation $|\Lambda_2|^2 \propto T^a$ with $a \approx 1$ is satisfied for wide temperature range: Such strong T -dependence of the charge-spin coupling Λ_2 is essential for realizing the orbital fluctuations, so it should be taken into account in the numerical calculation. As results, we obtain a crude approximation for the AL-VC $\tilde{X}_2^{\text{AL},c} \equiv 3U^4|\Lambda_2(\mathbf{0}; (0, \pi))|^2TC_2$ and show the result in Fig. 7 (d). This crude approximation qualitatively reproduces the exact numerical results for both FeSe and LaFeAsO given in Fig. 6 (c).

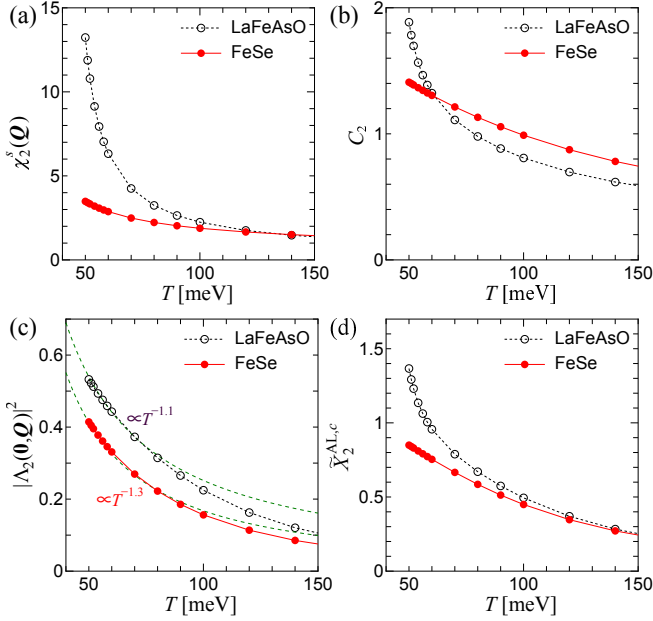


FIG. 7: **Origin of large AL-VC in FeSe.** (a) $\chi_2^s(\mathbf{Q})$, (b) $C_2 \equiv \sum_{\mathbf{q}} \chi_2^s(\mathbf{q})^2$, and (c) $|\Lambda_2|^2$ as functions of T in FeSe and LaFeAsO. (d) The approximate AL-VC for d_{xz} -orbital $\tilde{X}_2^{\text{AL},c} \equiv 3U^4|\Lambda_2(\mathbf{0}; (0, \pi))|^2TC_2$. In both FeSe and LaFeAsO, the obtained $\tilde{X}_2^{\text{AL},c}$ qualitatively agrees to the exact numerical calculations in Fig. 6 (c).

In summary, in both LaFeAsO and FeSe, strong orbital fluctuations are induced by AL-VC for the $d_{xz(yz)}$ -orbital, $X_{2(3)}^{\text{AL},c}(\mathbf{0})$. In FeSe, very small spin susceptibility χ_{max}^s is sufficient to realize the spin-fluctuation-driven orbital order, because of both the smallness of \bar{J}/\bar{U} and the largeness of C_2 . Strong T -dependence of Λ_2 is essential for realizing the orbital fluctuations due to AL-VC.

SC-VC analysis for FeSe: Smallness of the VC for the spin susceptibility

In the original SC-VC theory, the spin and charge susceptibilities are calculated self-consistently, by including the MT-VC and AL-VC for the spin and charge susceptibilities [13, 42]. The strong orbital fluctuations are induced by the charge-channel AL-VC in Fe-based SCs, Ru-oxides and cuprate SCs [13, 33, 51]. In the main text, we studied the eight-orbital $d-p$ Hubbard models for Fe-based SCs based on the SC-VC theory, by taking the charge-channel AL-VC into account self-consistently. The obtained $\chi^s(\mathbf{q})$ is equivalent to the RPA since the spin-channel VCs are dropped. Compared to the charge-channel AL-VC, the charge- and spin-channel MT-VCs are negligibly small. Also, the spin-channel AL-VC is found to be negligible in the two-orbital Hubbard model in Ref. [51].

Here, we study the FeSe model using the SC-VC method, by taking the MT-VC and AL-VC for both spin- and charge-channels in order to confirm the validity of the numerical study in the main text. The charge (spin) susceptibilities are

$$\hat{\chi}^{c(s)}(\mathbf{q}) = \hat{\Phi}^{c(s)}(\mathbf{q})(1 - \hat{\Gamma}^{c(s)}\hat{\Phi}^{c(s)}(\mathbf{q}))^{-1} \quad (8)$$

where $\hat{\Phi}^{c(s)}(\mathbf{q}) = \hat{\chi}^0(\mathbf{q}) + \hat{X}^{\text{MT},c(s)}(\mathbf{q}) + \hat{X}^{\text{AL},c(s)}(\mathbf{q})$. The spin-channel AL-VC is given as

$$\begin{aligned} X_{l,l';m,m'}^{\text{AL},s}(q) &= \frac{T}{2} \sum_p \sum_{a \sim h} \Lambda_{l,l';a,b;e,f}(q; p) \\ &\times [\{V_{a,b;c,d}^c(p+q)V_{e,f;g,h}^s(-p) \\ &+ V_{a,b;c,d}^s(p+q)V_{e,f;g,h}^c(-p)\}\Lambda'_{m,m';c,d;g,h}(q; p) \\ &+ 2V_{a,b;c,d}^s(p+q)V_{e,f;g,h}^s(-p)\Lambda''_{m,m';c,d;g,h}(q; p)] \end{aligned} \quad (9)$$

where $\Lambda''_{m,m';c,d;g,h}(q; p) \equiv \Lambda_{c,h;m,g;d,m'}(q; p) - \Lambda_{g,d;m,c;h,m'}(q; -p - q)$. Also, the expressions of the charge- and spin-channel MT-VCs are given in Ref. [42]. The double-counting second-order terms with respect to H^U in $\hat{X}^{\text{MT},s(c)} + \hat{X}^{\text{AL},s(c)}$ should be subtracted [42] to obtain reliable results.

Figures 8 (a) and (b) show the obtained $\chi^s(\mathbf{q})$ and $\chi_{x^2-y^2}^c(\mathbf{q})$, respectively, for $\bar{U} = 1.86$ eV ($r = 0.26$) at $T = 50$ meV. The Stoner factors are obtained as $\alpha_S = 0.907$ and $\alpha_C = 0.98$. The obtained VCs $X_2^{\text{MT+AL},s}(\mathbf{q})$ and $X_2^{\text{MT+AL},c}(\mathbf{q})$ for d_{xz} -orbital in the present self-consistent calculation are shown in Figs. 8 (c) and (d), respectively. Since $\hat{X}^{\text{MT+AL},s}(\mathbf{q})$ is very small, the obtained charge and spin susceptibilities are very similar to the results in Fig. 3 in the main text. Therefore, the validity of the numerical results in the main text is confirmed by performing the very time-consuming self-consistent calculation with respect to $\hat{X}^{\text{MT+AL},s,c}(\mathbf{q})$ and $\hat{\chi}^{s,c}(\mathbf{q})$.

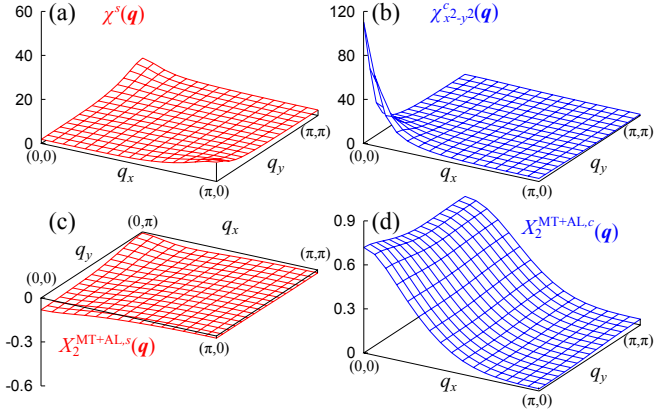


FIG. 8: **SC-VC theory with spin- and charge-channel VCs in FeSe model.** (a) $\chi^s(\mathbf{q})$ and (b) $\chi_{x^2-y^2}^c(\mathbf{q})$ given by the SC-VC theory, by calculating both spin- and charge-channel VCs self-consistently. The obtained results are quantitatively equivalent to Fig. 3 in the main text. This fact means that the VC for the spin channel is negligible. (c) $X_2^{MT+AL,s}(\mathbf{q})$ and (d) $X_2^{MT+AL,c}(\mathbf{q})$ obtained by the present self-consistent calculation.

Analysis of effective models of BaFe_2As_2 and NaFeAs

In the main text, we introduced the first principles models for LaFeAsO and FeSe , and analyzed these models by using the SC-VC method. Here, we also introduce the effective models for BaFe_2As_2 and NaFeAs , and analyze them using the SC-VC method.

In both BaFe_2As_2 and NaFeAs , the FSs have relatively large three-dimensional characters. In addition, the unfolding of the bandstructure in BaFe_2As_2 cannot be exactly performed because of its body-centered tetragonal crystal structure. Here, we introduce a simple effective BaFe_2As_2 TB model $H_{\text{BaFe}_2\text{As}_2}^0$ by magnifying the size of the d_{xy} -orbital hole-FS around $\mathbf{q} = (\pi, \pi)$ in the LaFeAsO unfolded model, in order to reproduce the ARPES bandstructure in Ba122 compounds. As for NaFeAs , we just use H_{LaFeAsO}^0 as an effective NaFeAs TB model, *e.g.*, $H_{\text{NaFeAs}}^0 = H_{\text{LaFeAsO}}^0$, because of the fact that the FSs in NaFeAs in the $k_z = 0$ plane are similar to the FSs in LaFeAsO . We use H_{NaFeAs}^U in place of H_{LiFeAs}^U given in Ref. [30].

The bandstructures and the FSs of the effective TB models for BaFe_2As_2 and NaFeAs are shown in Figs. 9 (a)-(c). Here, we perform the SC-VC analysis for the models $H_M = H_M^0 + rH_M^U$ ($M = \text{BaFe}_2\text{As}_2, \text{NaFeAs}$), where $r (< 1)$ is the reduction parameter. We choose the parameter r to satisfy the charge Stoner factor is $\alpha_C = 0.98$; The obtained T -dependences of the spin and charge Stoner enhancement factors, $S_S \equiv (1 - \alpha_S)^{-1}$ and $S_C \equiv (1 - \alpha_C)^{-1}$ respectively, are shown in Fig. 9 (d) and (e). As for BaFe_2As_2 , both spin and orbital fluctu-

ations strongly develop at $T \sim 50$ meV in the case of

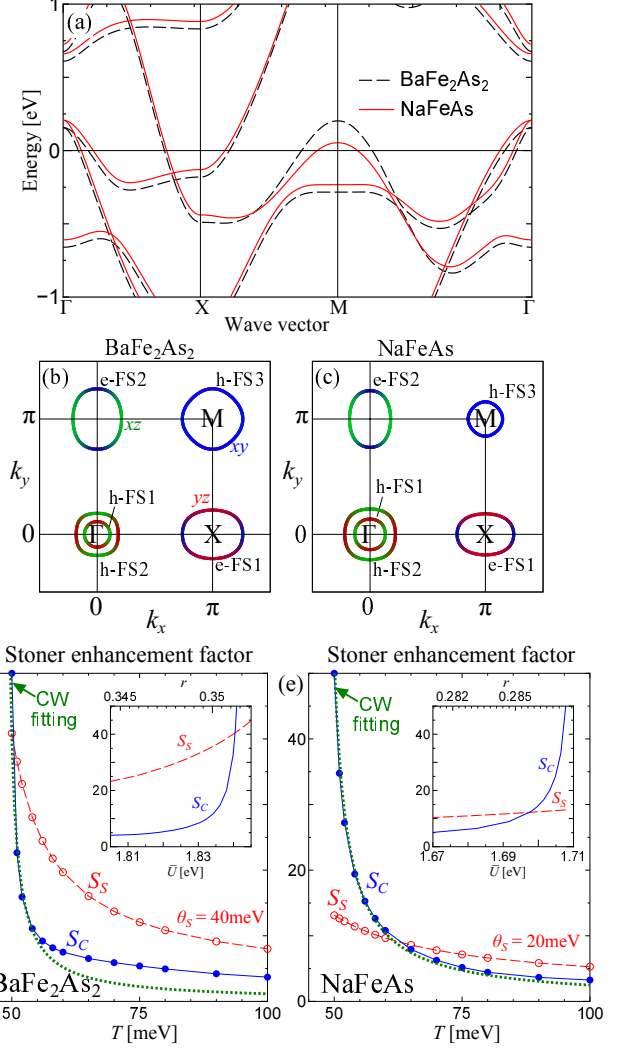


FIG. 9: **Analyses of BaFe_2As_2 and NaFeAs models using the SC-VC theory.** (a) Bandstructures of $H_{\text{BaFe}_2\text{As}_2}^0$ and H_{NaFeAs}^0 . (b) FSs of $H_{\text{BaFe}_2\text{As}_2}^0$ and (c) FSs of H_{NaFeAs}^0 . (d) T -dependences of the spin (charge) Stoner enhancement factors $S_S(S_C)$ obtained in $H_{\text{BaFe}_2\text{As}_2}^0$. (Inset) The \bar{U} -dependences of the Stoner enhancement factors. (e) Spin and charge Stoner enhancement factors in H_{NaFeAs}^0 .

$r = 0.36$. This result is consistent with experimental relation $T_{\text{mag}} \approx T_{\text{str}}$ in BaFe_2As_2 . As for NaFeAs , only orbital fluctuations strongly develop whereas spin fluctuations remain moderate at $T \sim 50$ meV in the case of $r = 0.287$. This result is consistent with experimental results in NaFeAs [49], in which $T_{\text{mag}} (= 40\text{K})$ is more than ten Kelvin smaller than $T_{\text{str}} (= 53\text{K})$. Thus, normal-state phase diagrams in BaFe_2As_2 and NaFeAs are well explained by analyzing their effective Hamiltonians using the SC-VC method.